Iran University of Science and Technology

International Journal of

Railway Research

ISSN: 2423-3838

Investigation of a rectangular energy absorber with a near-ovoid internal lattice structure for use in a train buffer system

Hossein Fakhri Vayqan[1], Pouyan Tahouneh [1], Parisa Hosseini Tehrani [1*]

[1] School of Railway Engineering, Iran University of Science and Technology, Tehran, Iran

16846-13114, Iran, Hosseini_tiust@iust.ac.ir

ARTICLE INFO

Article history:

Received:04.05.2024

Accepted: 05.10.2024

Published: 14.10.2024

Keywords:

Crashworthiness

Thin-walled tube

Lattice structure

Railway

Offset loading

A B S T R A C T

In this study, a thin-walled tube with a near-ovoid-lattice internal cell (OLC) made of stainless steel is introduced. The crashworthiness performance of the presented structure in railway applications is investigated. The crash behavior of the OLC structure is simulated using the explicit finite element code LS-DYNA under various loading scenarios, including axial, offset, and oblique loading. To validate these results, simulations of a rectangular thin-walled tube with diaphragms are conducted, and the numerical outcomes are compared against existing experimental data for accuracy. Based on the results, the OLC design exhibits enhanced energy absorption capabilities. By integrating the lattice structure into the crashworthy configuration, a significant increase of 36.24% in energy absorption and a substantial 11.94% rise in specific energy absorption are observed. Moreover, a notable 25.91% improvement is seen in the crushing force efficiency, indicating a more balanced distribution of force with a flatter curve due to a greater mean force than peak force. Additionally, consistent crushing behavior up to 40 mm under offset loading and 15 degrees under oblique loading in the OLC design is seen, and its energy absorption is maintained at a constant level.

1. Introduction

Improved safety performance in accidents is a critical concern across industries such as railways, automobiles, aerospace, etc. Ensuring passenger safety and reducing injuries during railway accidents have long been focal points in the transportation sector. Extensive research has been dedicated to designing and manufacturing energy absorbers to enhance crashworthiness abilities. To absorb more kinetic energy during the crash and achieve a higher level of crashworthiness, thin-walled structures such as tubes [1-5], honeycombs [6, 7], and lattices [8-10] made of lightweight materials such as aluminum alloys [11-13], high-strength steels [14, 15], composites [16-18], and foams [19, 20] are introduced. Langseth and Hopperstad [21] conducted an experimental study to examine the behavior of aluminum alloy (AA6060) square thin-walled tubes under dynamic and quasi-static axial loading conditions. They studied different variables such as wall thickness and impact speed. They observed a state of progressive symmetric deformation independent of the mentioned variables in the structure of the thin wall tubes. Additionally, in another study [22], they confirmed the experimental findings from the previous study through simulations conducted in LS-DYNA. Hosseini-Tehrani et al. [23] numerically conducted the crushing of polygonal thin-walled tubes. They found that the octagonal cross-section may show better energy absorption characteristics under axial and

*Corresponding author
Email address: Hosseini_t@iust.ac.ir

[DOI: 10.22068/ijrare.351]

oblique loading. In a separate study [24], the authors investigated the crushing behavior of the nose of high-speed trains when subjected to axial loads. They found that the foam between the inner and outer layers could significantly increase the energy absorption.

According to the railway standard EN15227 [25], during a train accident, derailment and climbing occur due to vertical displacements and forces caused by displacements between contact points of the interface. The inertial forces are related to reducing the speed and acceleration of the vehicle. In EN15227 [25], there is a specified criterion for the primary constraint in scenario 1 as follows: when there is an initial vertical offset of 40 mm at the impact point, contact between at least one wheelset of each bogie and the track should be sustained during the collision simulation. Han and Park [26] investigated the effect of oblique loading on the crushing behavior of a square column through experiments and numerical simulations. The results showed that bending collapse occurs when the loading angle increases more than the critical load angle. Gao et al. [27] by examining the energy absorption of normal tubes and tubes with a diaphragm showed that the diaphragm increases the stability and controls the formation of folds. Dong et al. [28] found the effective performance of diaphragms in the collision behavior of two-tube structures through a numerical study. Xu et al. [29] investigated the crash performance of an innovative axisymmetric rectangular tube with diaphragms subjected to axial quasi-static loads using a combination of experimental tests and numerical simulations. Their primary focus was on studying the impact of two different wall and diaphragm thicknesses on the energy absorption characteristics and the identification of optimal design configurations. They found that the uniform-thickness tube with diaphragms demonstrated effective energy absorption. Xu et al. [30] experimentally and numerically conducted investigations on the crashworthiness of a tube with uniform thickness and diaphragms under various offset loads. They found that thickness settings significantly affected crash performance at a given offset distance, and finally, the non-uniform thickness axisymmetric rectangular tube compared to the uniform thickness tube had higher impact capability.

In this study, the crash performance of a rectangular thin-walled tube with a near-ovoid-lattice internal cell (OLC) made of stainless steel is examined. The performance of this design under axial, offset, and oblique loadings in quasi-static conditions is evaluated. Numerical modeling of OLC adapted for railway applications is presented and discussed. The LS-DYNA explicit nonlinear finite element analysis code is employed to develop the numerical simulations. To validate the accuracy of the FE modeling, comparison is made with the numerical results and experimental data [29].

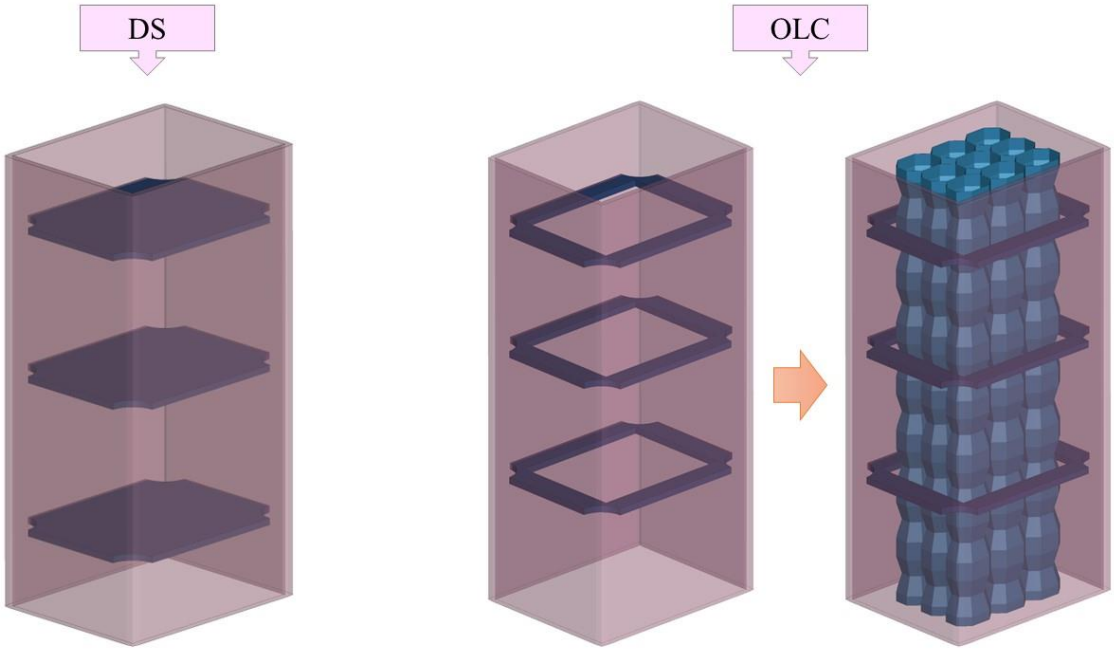

Figure 1. Schematic view of DS & OLC.

[DOI: 10.22068/ijrare.351]

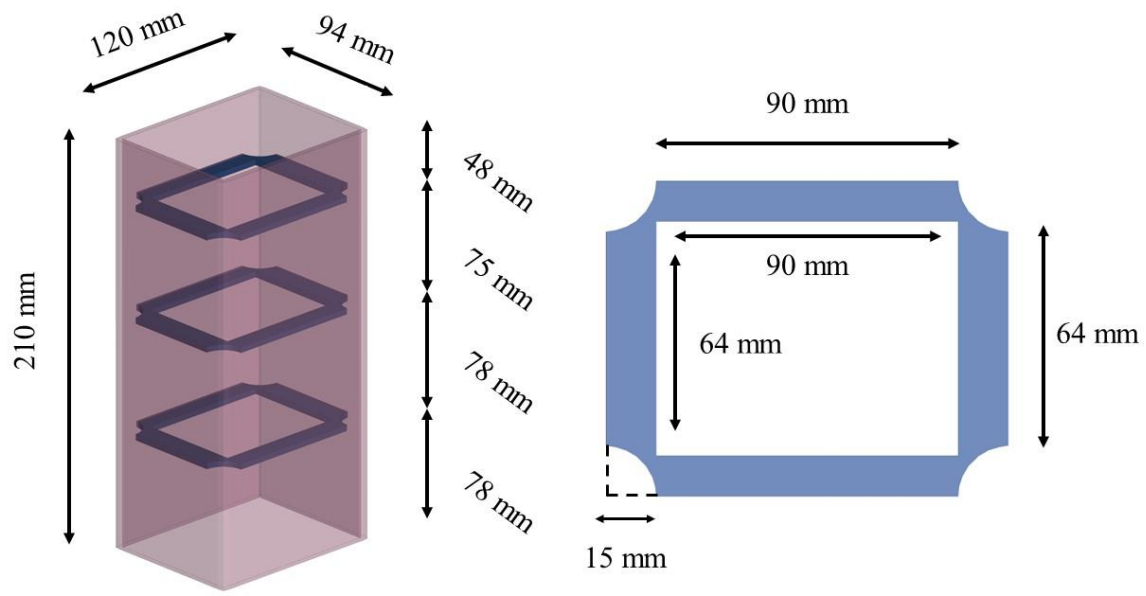

Figure 2. Dimensions of the tube with trimmed diaphragms.

2. Model design and numerical methods

2.1. Explanation of geometry

In this work, the crashworthiness response of the two structures shown in Figure 1 is compared. The first one is a rectangular thin-wall tube with diaphragms (DS), and the second one is a rectangular thin-wall tube with trimmed diaphragms and a near-ovoid-lattice internal cell (OLC). In both structures, the diaphragms are positioned horizontally at varying distances, and in OLC, a near-ovoid-lattice internal cell is placed inside trimmed diaphragms, as shown in Figure 2. The thicknesses of the tube and diaphragms are 4 mm and 1 mm. Figure 2 shows the diaphragm dimensions. The first diaphragm is located 48 mm from the top; the second diaphragm is located 75 mm from the first diaphragm; and the third diaphragm is located 78 mm from the second diaphragm. The lattice structure is positioned vertically inside the tube, at the center of the trimmed diaphragms. The dimensions of one cell of the lattice structure

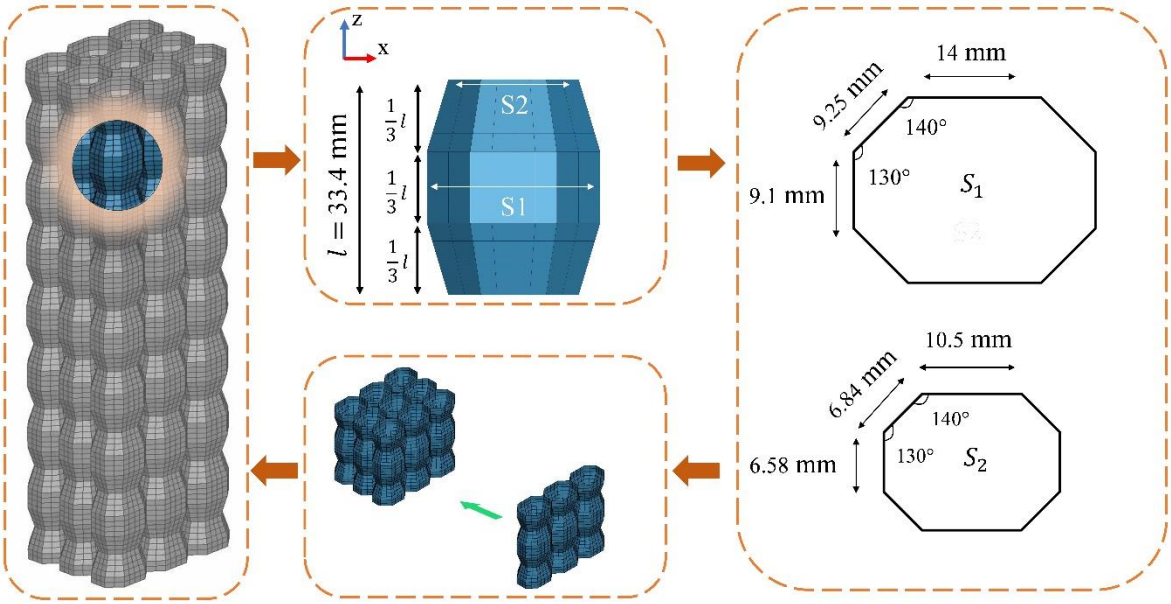

Figure 3. Steps of simulating near-ovoid-lattice internal cell (lattice structure).

[DOI: 10.22068/ijrare.351]

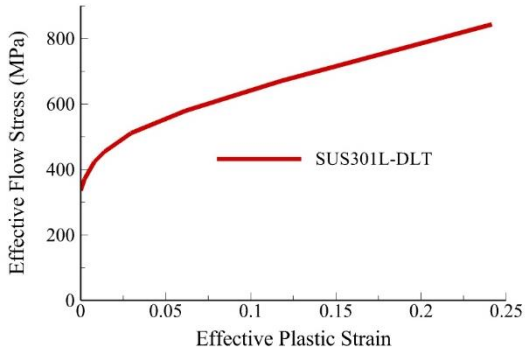

Figure 4. Stress-strain curve for stainless steel material SUS301L-DLT [29].

component and their layout are depicted in Figure 3. In the industry, these lattice structures can be fabricated in various sections and assembled through the laser beam welding (LBW) process.

2.2. Numerical Models

In this study, the LS-DYNA explicit nonlinear finite element analysis code is employed to generate numerical models. The thin wall, diaphragms, and lattice structure are represented using four-node Belytschko-Tsay shell elements, while the impactor was modeled with hexahedral solid elements. As illustrated in Figure 5, a series of simulations with varying element sizes were conducted to examine the mesh sensitivity. The results demonstrated that an element size of 3×3 mm represents the optimal mesh size. Moreover, the element size of the impactor is considered 10 mm and defined as a rigid body. The masses of the DS and OLC are 4.7 and 5.8 kg, respectively. All of the designed models are constructed from stainless steel SUS301L-DLT [6]. The mechanical properties of these materials and their true stress versus plastic strain curves are demonstrated in Table 1 and Figure 4, respectively. The material properties from MAT#24 in the LS-DYNA material library are employed to define the material characteristics. MAT#20 features are also employed to define the impactor material. The stress-strain curve (Figure 4) is applied to these material models. All simulations are conducted under quasi-static conditions, and the strain rate effect is neglected. The impactor moves forward with a constant velocity of 1 m/s in the through down while the bottom nodes are fixed (Figure 6).

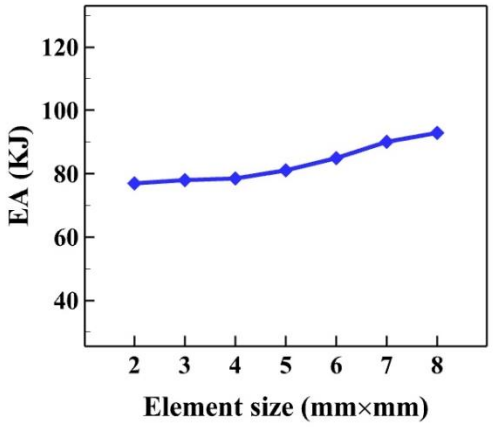

Figure 5. The mesh sensitivity analysis for the tube with trimmed diaphragms.

The "AUTOMATIC_SURFACE_TO_SURFACE" contact type in LS-Dyna is chosen for establishing contact between the impactor and the absorber structure, as well as for internal contacts between the DS and the lattice structure. The static coefficient of friction is specified as 0.3, while the dynamic coefficient of friction is defined as 0.2 [29].

Table 1. Mechanical Properties of stainless steel SUS301L-DLT [29].

Mechanical parameters	SUS301L-DLT
Density (kg/m3)	7850
Young's modulus (GPa)	206
Poisson's ratio	0.3
Yield stress (MPa)	335

2.3. Crashworthiness criteria

The crashworthiness criteria, such as maximum crushing force, average crushing force, energy absorption, and specific energy absorption, are used to evaluate the considered structures. The main criteria are defined as follows:

Peak crushing force (PCF) is the maximum peak force in the crushing process of a structure. The initial peak crushing force is abbreviated as IPCF. Energy Absorption (EA) is the absorbed energy in the crushing process defined as:

[DOI: 10.22068/ijrare.351]

$$EA = \int_0^{\delta_{max}} F(\delta)d\delta \quad (1)$$

where δ_{max} is the effective deformation distance, and the crushing force as a function of displacement δ during the crushing process is defined as $F(\delta)$.

Mean crushing force (MCF) is defined as:

$$MCF = \frac{EA}{\delta_{max}} \quad (2)$$

Specific energy absorption (SEA) is defined as:

$$SEA = \frac{EA}{m} \quad (3)$$

where m is the mass of the energy absorber. Crushing Force Efficiency (CFE) is the difference between PFC and MFC and is quantified by calculating the ratio between them, which ranges from 0 to 1. A higher CFE indicates a better energy absorber structure. CEF is defined as:

$$CFE = \frac{MCF}{PCF} \quad (4)$$

3. Numerical Results

3.1. FEM validation and numerical details

To evaluate the simulation results, the LS-DYNA numerical results are validated with the experimental data published by Xu et al. [29]. They investigated the crash performance of an axisymmetric rectangular tube with diaphragms. The simulation was carried out until the crushing distance of 200 mm and with a constant velocity of 1 m/s. The numerical results closely predicted the deformation and shape of the folds and the forced displacement response, as demonstrated in Figure 7 and Table 2.

Table 2. Simulation results for a rectangular DS and comparison with experimental results [29].

	Present study	Xu et al. 2019	Error %
EA(KJ)	77.9	76.77	1.47
IPCF(KJ)	702.98	695.79	1.03
MCF(KJ)	389.5	383.85	1.47
δ_{max}(mm)	200	200	-

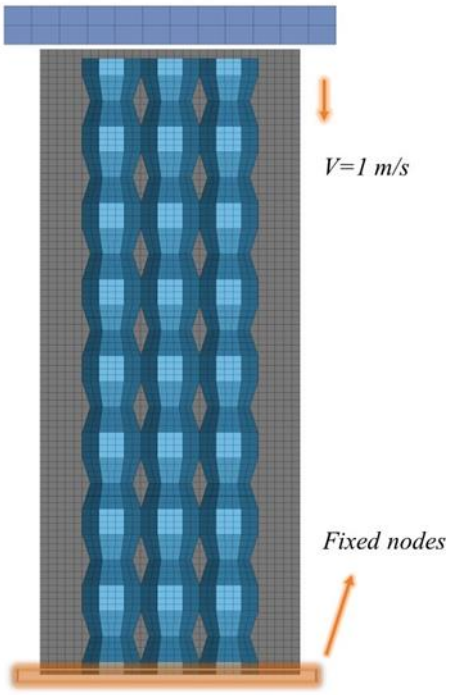

Figure 6. Section view of FE model under quasi-static loading situation.

In this stage, a rectangular thin-walled tube with diaphragms (DS) and a rectangular thin-walled tube with trimmed diaphragms containing a near-ovoid-lattice internal cell (OLC) are compared. To evaluate the crash performance of the OLC, Figure 8 and Table 3 display the force-displacement response and energy absorption and performance indicators of the two considered models (OLC AND DS). The effective crushing length should be considered to check the energy absorption of structures. Theoretically, as the crushing distance extends, the deformation efficiency is expected to increase and peak at the effective deformation distance. Therefore, the effective crushing length is 180 mm for OLC and 200 mm for DS. As shown in Table 3, for OLC the EA increases by 36.23% considering the effective length, and the SEA also increases by almost 12%.

The force-displacement graph of OLC is flatter, and the mean and peak crushing force in this design are closer to each other in comparison to the DS model. This phenomenon results in better energy absorption characteristic of OLC. Figure 9 depicts the fold formation and crushing deformation of the OLC. Diaphragms are placed

[DOI: 10.22068/ijrare.351]

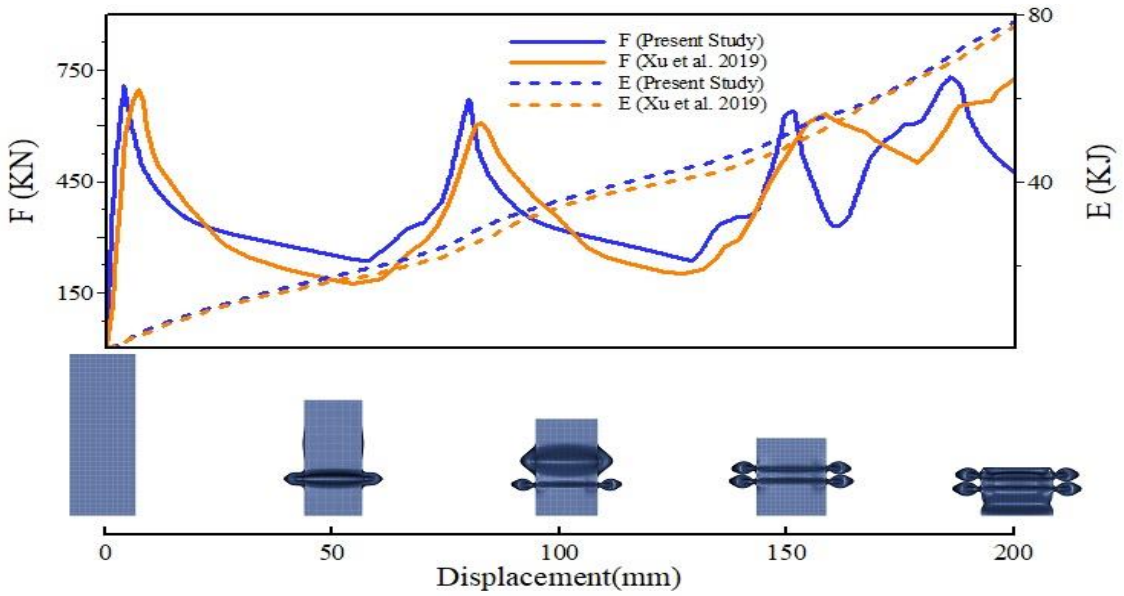

Figure 7. Comparison of force-displacement curves between the experimental results of Xu et al. [29] and simulation results of the present study subjected to quasi-static loading.

within the tube to control fold formation and enhance structural stability during crushing.

The OLC includes three trimmed diaphragms positioned at specific intervals, as shown in Figure 3. Tube folds are more easily created when diaphragms are spaced farther apart. Cutting the diaphragms reduces their stiffness and resistance to deformation, but when placed at significant distances, they conduct the folding process. The first fold forms between the lowest diaphragm and the tube end. Subsequently, as the striker descends, two other folds develop between the middle and bottom trimmed diaphragms (one inward and one outward). Another fold forms between the upper and middle diaphragms. Considering the near-ovoid lattice cell crushing, it is observed that initially, areas with smaller cross-sections are crushed. As the crushing progresses, each piece of lattice structure transitions from a near-ovoid-shaped configuration to a cylindrical one. Notably, the energy absorption during the initial deformation phase is lower than when the cylindrical shape is fully formed, leading to a distinct two-stage timing in the crushing process. Furthermore, apart from absorbing axial energy from the impactor, the lattice structure adds complexity to the formation of tube folds. As a result, energy absorption by OLC increases both the resistance to crushing and the deformation of the structure.

3.2. Crashing analysis of crashworthy structure under offset & oblique loading

In this section, the performance of the OLC structure is examined under various conditions, including offset and oblique loading. According to the EN 15227 [25], the absorber must retain its energy absorption characteristics even under offset loading up to 40 mm. To address this requirement, the force-displacement response of the OLC is analyzed for three different offsets: 20 mm, 40 mm, and 60 mm (Figure 10). Based on Table 4, the OLC maintained consistent energy absorption levels as the loading offset distance increased to 40 mm.

Table 3. Performance comparison of OLC and DS.

	EA (KJ)	SEA (KJ/Kg)	MCF (KJ)	PCF (KJ)	CFE %	δ_{max}(mm)
OLC	107	18.45	594.61	855.2	69.52	180
DS	78.56	16.48	392.8	711.4	55.21	200
Difference%	36.24	11.94	51.37	20.21	25.91	-

[DOI: 10.22068/ijrare.351]

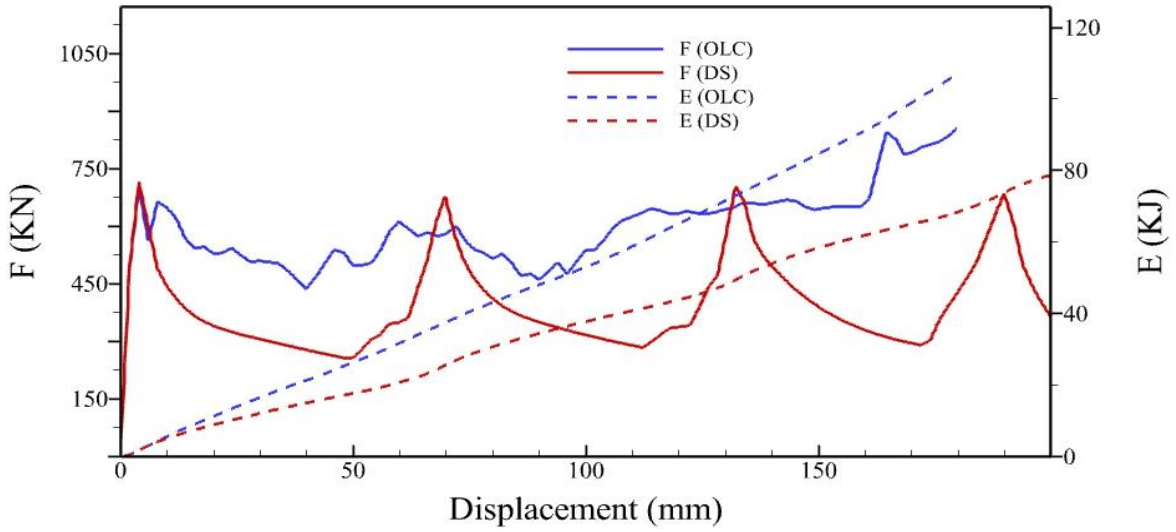

Figure 8. Force, energy-displacement responses of crushing OLC and DS under quasi-static impact.

Table 3. Energy absorption of OLC under offset and oblique loading conditions.

Loading		EA
	γ°	(KJ)
Oblique	0	107.03
	5	102.04
	10	100.47
	15	95.24
	20	76.44
	d (mm)	(KJ)
Offset	0	107.03
	20	102.68
	40	111.71
	60	27.85

However, a 4% decrease is observed at a 20 mm offset distance, while a 4% increase occurred at 40 mm. Consequently, the OLC complies with standard requirements. Figure 11 illustrates the deformation of the OLC under offset and oblique loading conditions. At a 60 mm offset distance, energy absorption efficiency of the OLC structure as the loading angle decreased.

Furthermore, Figure 11 demonstrates that with a loading angle of 20 degrees, the OLC experienced bending and sliding that disrupted its energy absorption capabilities. In oblique loading scenarios, four angles of 5, 10, 15, and 20 degrees are tested to evaluate the OLC's performance. Table 4 indicates a decrease in the energy absorption efficiency of the OLC structure as the loading angle increased.

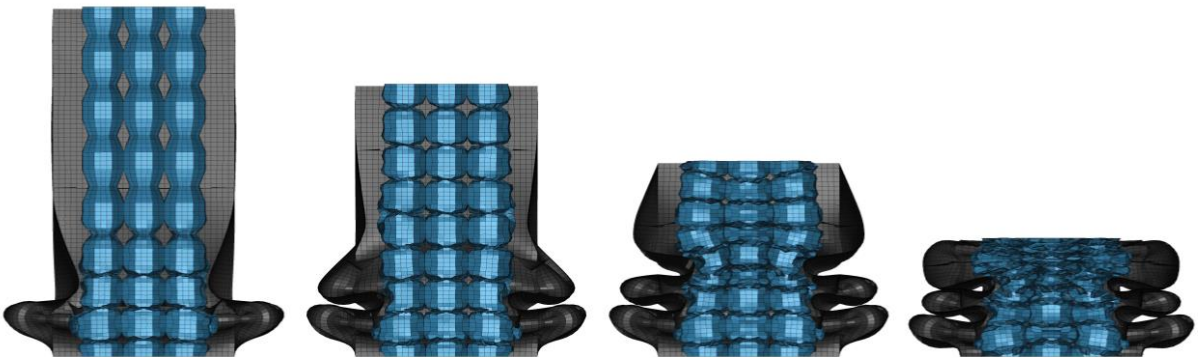

Figure 9. Front section view of deformation of the OLC, from left to right: 50-, 100-, 150- and 200-mm displacement.

[DOI: 10.22068/ijrare.351]

Furthermore, Figure 10 demonstrates that with a loading angle of 20 degrees, the OLC experienced bending and sliding that disrupted its energy absorption capabilities.

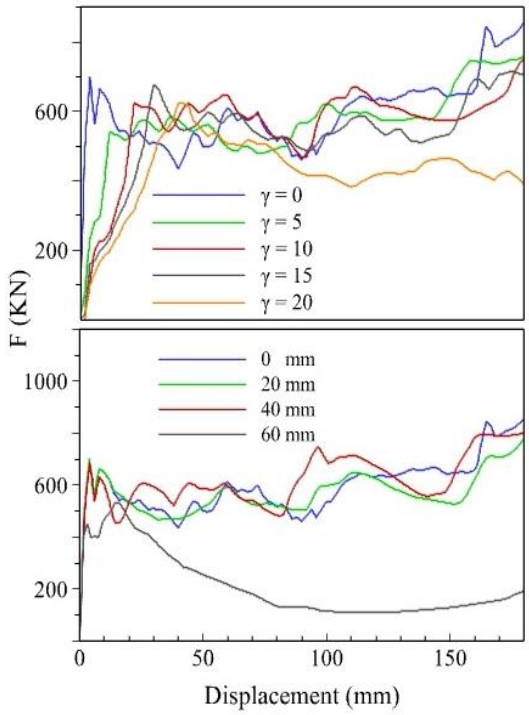

Figure 10. Force-displacement response of OLC under oblique & offset loadings.

4. Conclusion

A thin-walled tube with near-ovoid-lattice internal cells (OLC) has been proposed as an energy absorber for railway applications. The suitability of this design is explored by the finite element method (FEM) to evaluate the energy absorption response and the deformation mechanism. Furthermore, non-axial compression situations are demonstrated to assess the ability of OLC to withstand the offset and oblique loading in a railway context. The subsequent findings are derived from this research:

(1) The lattice internal structure adds complexity to tube deformation and increases energy absorption. The use of the OLC increases the resistance to both the crushing and folding processes.
(2) Using the lattice internal structure (OLC) increases EA, SEA, PCF, MFC, and CFE by 36.23%, 12%, 20.21%, 51.37%, and 25.29%, respectively, compared to DS.
(3) The energy-absorbing capacity of the OLC decreases after deforming 60 mm under an offset load of 20 degrees. However, the OLC remains stable under an offset load of up to 40 mm of deformation and an oblique load of up to 15 degrees.

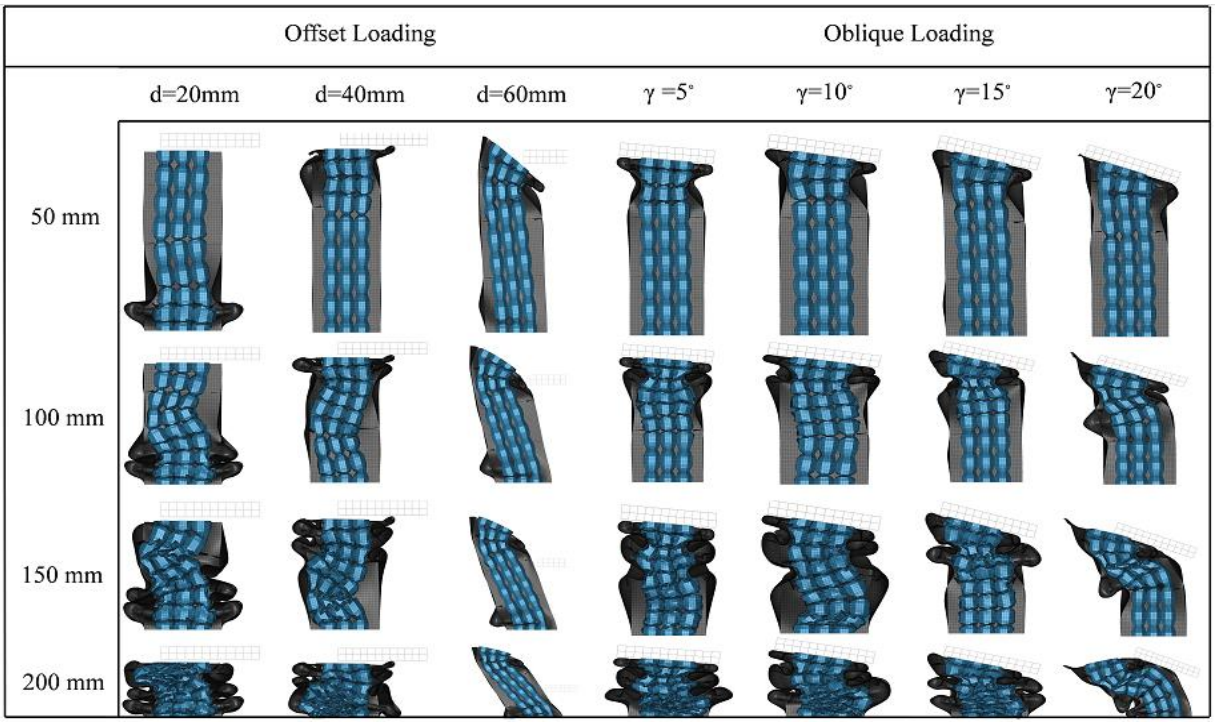

Figure 11. Crashworthy structure deformation under different loading situations.

[DOI: 10.22068/ijrare.351]

References

[1] T. Zhang, Z. Liu, S. Li, J. Lei, and Z. Wang, "Dynamic response and energy absorption performance of aluminum foam-filled sandwich circular tubes under internal blast loading," International Journal of Impact Engineering, vol. 173, (2023), pp. 104458.

[2] M. R. Faraz, H. Ahmadi, G. Liaghat, S. Vahid, O. Razmkhah, and A. Tarafdar, "Energy absorption assessment of bio-mimicked hybrid Al/PP sandwich tube: Experimental and Numerical Investigation," Thin-Walled Structures, vol. 181, (2022), pp. 110116.

[3] Z. Song et al., "Energy absorption of metal-composite hybrid tubes with a diamond origami pattern," Thin-Walled Structures, vol. 180, (2022), pp. 109824.

[4] X.-G. Lian, L.-X. Lu, and L. Pan, "Investigation of energy absorption characteristics of circular paper tubes under axial impact loading," International Journal of Impact Engineering, vol. 165, (2022), pp. 104210.

[5] P. Ataabadi, D. Karagiozova, and M. Alves, "Crushing and energy absorption mechanisms of carbon fiber-epoxy tubes under axial impact," International Journal of Impact Engineering, vol. 131, (2019), pp. 174-189.

[6] J. Zhang and G. Lu, "Dynamic tensile behaviour of re-entrant honeycombs," International journal of impact engineering, vol. 139, (2020), pp. 103497.

[7] Y. Duan et al., "Crushing behavior of honeycomb vs. foam under combined shear-compression loading," International Journal of Impact Engineering, vol. 146, (2020), pp. 103696.

[8] S. E. Alkhatib, A. Karrech, and T. B. Sercombe, "Isotropic energy absorption of topology optimized lattice structure," Thin-Walled Structures, vol. 182, (2023), pp. 110220, 2023.

[9] H. Zhu, P. Wang, D. Wei, J. Si, and Y. Wu, "Energy absorption of diamond lattice cylindrical shells under axial compression loading," Thin-Walled Structures, vol. 181, (2022), pp. 110131.

[10] G. Zheng et al., "Investigation into multiaxial mechanical behaviors of Kelvin and Octet-B polymeric closed-cell foams," Thin-Walled Structures, vol. 177, (2022), pp. 109405, 2022.

[11] R. Dubey, R. Jayaganthan, D. Ruan, N. Gupta, N. Jones, and R. Velmurugan, "Energy absorption and dynamic behaviour of 6xxx series aluminium alloys: A review," International Journal of Impact Engineering, vol. 172, (2023), pp. 104397.

[12] V. Vilamosa, A. H. Clausen, T. Børvik, S. Skjervold, and O. S. Hopperstad, "Behaviour of Al-Mg-Si alloys at a wide range of temperatures and strain rates," International Journal of Impact Engineering, vol. 86, (2015), pp. 223-239.

[13] M. Jobba, R. Mishra, and M. Niewczas, "Flow stress and work-hardening behaviour of Al–Mg binary alloys," International Journal of Plasticity, vol. 65, (2015), pp. 43-60.

[14] C. Fan, Z. Xu, Y. Han, Y. Liu, and F. Huang, "Loading rate effect and failure mechanisms of ultra-high-strength steel under mode II fracture," International Journal of Impact Engineering, vol. 171, (2023), pp. 104374.

[15] Z. Wang and M. Huang, "Optimising the strength-ductility-toughness combination in ultra-high strength quenching and partitioning steels by tailoring martensite matrix and retained austenite," International Journal of Plasticity, vol. 134, (2020), pp. 102851, 2020.

[16] J. Huang et al., "A new partially-infused fiber reinforced thermoplastic composite for improving impact resistance," International Journal of Impact Engineering, vol. 168, (2022), pp. 104293.

[17] C. S. Yerramalli, C. Sumant, R. K. Prusty, and B. C. Ray, "Finite element modelling and experimentation of plain weave glass/epoxy composites under high strain-rate compression loading for estimation of Johnson-Cook model parameters," International Journal of Impact Engineering, vol. 167, (2022), p. 104262, 2022.

[18] J. Xie et al., "Mechanics of textiles used as composite preforms: A review," Composite structures, vol. 304, (2023), pp. 116401.

[19] F. Rahimidehgolan, Y. Liu, and W. Altenhof, "Experimental, numerical and analytical investigations on the elevated strain rate compressive behavior of high-performance

[DOI: 10.22068/ijrare.351]

PES foam up to 200 s− 1," International Journal of Impact Engineering, vol. 161, (2022), pp. 104088.

[20] X. Pang and H. Du, "Dynamic characteristics of aluminium foams under impact crushing," Composites Part B: Engineering, vol. 112, (2017), pp. 265-277.

[21] M. Langseth and O. Hopperstad, "Static and dynamic axial crushing of square thin-walled aluminium extrusions," International Journal of Impact Engineering, vol. 18, no. 7-8, (1996), pp. 949-968.

[22] M. Langseth, O. Hopperstad, and T. Berstad, "Crashworthiness of aluminium extrusions: validation of numerical simulation, effect of mass ratio and impact velocity," International Journal of Impact Engineering, vol. 22, no. 9-10, (1999), pp. 829-854.

[23] P. Hosseini-Tehrani and S. Pirmohammad, "Collapse study of thin-walled polygonal section columns subjected to oblique loads," Proceedings of the Institution of Mechanical Engineers, Part D: Journal of Automobile Engineering, vol. 221, no. 7, (2007), pp. 801-810.

[24] P. Hosseini-Tehrani and A. Nankali, "Study on characteristics of a crashworthy high-speed train nose," International Journal of Crashworthiness, vol. 15, no. 2, (2010), pp. 161-173.

[25] Railway applications - Crashworthiness requirements for railway vehicle bodies. EN 15227 , January 2008.

[26] D. Han and S. Park, "Collapse behavior of square thin-walled columns subjected to oblique loads," Thin-Walled Structures, vol. 35, no. 3, (1999), pp. 167-184.

[27] G. Gao, H. Dong, and H. Tian, "Collision performance of square tubes with diaphragms," Thin-Walled Structures, vol. 80, (2014), pp. 167-177.

[28] H.-p. Dong, G.-j. Gao, S.-c. Xie, and J. Li, "Collision performance of bitubular tubes with diaphragms," Journal of Central South University, vol. 22, no. 9, (2015), pp. 3657-3665.

[29] P. Xu et al., "Parameter study and multi-objective optimisation of an axisymmetric rectangular tube with diaphragms for subways," Thin-Walled Structures, vol. 136, (2019), pp. 186-199.

[30] K. Xu et al., "Crashworthiness optimisation for the rectangular tubes with axisymmetric and uniform thicknesses under offset loading," Structural and Multidisciplinary Optimization, vol. 62, (2020), pp. 957-977.

[DOI: 10.22068/ijrare.351]